Fabrication methods and performance of low-permeability microfluidic components for a miniaturized wearable drug delivery system

Fabrication Methods and Performance of Low-Permeability Microfluidic Components for a Miniaturized Wearable Drug Delivery System

Mark J. Mescher, Erin E. Leary Swan, Jason Fiering, Maria E. Holmboe, William F. Sewell, Sharon G. Kujawa, Michael J. McKenna, and Jeffrey T. Borenstein

***Abstract*—In this paper, we describe low-permeability components of a microfluidic drug delivery system fabricated with versatile micromilling and lamination techniques. The fabrication process uses laminate sheets which are machined using XY milling tables commonly used in the printed-circuit industry. This adaptable platform for polymer microfluidics readily accommodates integration with silicon-based sensors, printed-circuit, and surface-mount technologies. We have used these methods to build components used in a wearable liquid-drug delivery system for *in vivo* studies. The design, fabrication, and performance of membrane-based fluidic capacitors and manual screw valves provide detailed examples of the capability and limitations of the fabrication method. We demonstrate fluidic capacitances ranging from 0.015 to 0.15 μL/kPa, screw valves with on/off flow ratios greater than 38 000, and a 45$\times$ reduction in the aqueous fluid loss rate to the ambient due to permeation through a silicone diaphragm layer. [2008-0148]**

***Index Terms*—Fluidics, implantable biomedical devices, micromachining, permeability, polyimide films, printed-circuit fabrication.**

I. Introduction

EXISTING techniques for delivery of drugs to the inner ear are extremely limited due to challenges specific to the inaccessibility and sensitivity of cochlear structures. Methods including controlled-release polymers and hydrogels are being explored but do not allow for high precision or control over pharmacokinetic profiles. Current approaches such as miniosmotic pumps operate for short durations and, therefore, do not address the principal clinical opportunities related to the long-term delivery of regenerative compounds to treat sensorineural hearing loss [1]. To address this need, we are developing a novel microfluidic high-precision delivery system, described elsewhere [2], [3], with polymer microfabricated components.

Implantable or wearable active microfluidic drug delivery systems require integration of a fluid delivery module with miniaturized electronics, power supply, and biocompatible packaging for long-term safe and reliable operation. A wide variety of fabrication techniques have been explored and developed for producing microfluidic components and systems [4]. Cast molding [5] and associated soft lithography techniques [6], patterning of spin-on polymers [7], embossing [8], [9], and combined methods [10]–[12] are popular. However, these methods have been generally developed for short-term or single-use devices. Furthermore, many of these polymer prototyping approaches cannot be seamlessly integrated using current techniques for electronics packaging. The stringent size and reliability constraints imposed on an ultraminiaturized drug delivery system call for a hybrid fabrication platform that is highly stable and can incorporate both fluidic and electronic elements.

In view of these requirements, microfabrication using polyimide films represents a potential platform for drug delivery systems. Because of its combination of chemical inertness, high temperature tolerance, and robust mechanical properties, this material is routinely used in mesoscale flex circuits and electronics packaging and has also been used for polymer microelectromechanical-systems (MEMS) applications and biosensors [13]–[16].

Polyimide has also been used specifically for microfluidics. Pacific Northwest National Laboratory researchers have done extensive development of complex fluidic systems which are integrated with actuators and electronics [17]. They used an excimer laser to through-machine sheets and, then, laminated them to construct microfluidic structures. Previously, we have used similar laser-machining techniques to construct complex microfluidic devices, for example, a closed-loop flow controller implemented with an anemometer-based flow sensor and an electronically controlled microvalve [18]. We have also implemented new fabrication methods, including reactive-ion-etch thinning of film adhesives (to minimize dimensional changes in channels which occur during lamination) and controlled partial-depth laser machining of laminate sheets [19]. This latter capability is advantageous because depth dimensions, e.g., channel depth and valve-seat height, are not limited to available stock sheet thicknesses.

Manuscript received June 11, 2008; revised October 23, 2008. First published April 21, 2009; current version published June 3, 2009. This work was supported by the National Institute of Deafness and other Communication Disorders (NIDCD) under Grant 5 R01 DC 006848-02. Subject Editor Y. B. Gianchandani.

M. J. Mescher, J. Fiering, M. E. Holmboe, and J. T. Borenstein are with Charles Stark Draper Laboratory, Cambridge, MA 02139 USA (e-mail: mmescher@draper.com; jfiering@draper.com; mholmboe@draper.com; jborenstein@draper.com).

E. E. Leary Swan is with Charles Stark Draper Laboratory, Cambridge, MA 02139 USA, and also with the Department of Mechanical Engineering, Massachusetts Institute of Technology, Cambridge, MA 02139 USA (e-mail: eswan@draper.com).

W. F. Sewell, S. G. Kujawa, and M. J. McKenna are with the Massachusetts Eye and Ear Infirmary, Boston, MA 02114 USA, and also with Harvard Medical School, Boston, MA 02115 USA (e-mail: wfs@epl.meei.harvard.edu).

Digital Object Identifier 10.1109/JMEMS.2009.2015484

Despite its advantages, fabrication with polyimide sheets presents challenges, particularly when rapid and frequent design revisions are desired. Laser-machining systems, while versatile, are typically expensive to acquire and maintain, and die-tooling costs can be prohibitive. In contrast, XY routing tables used for printed-circuit-board (PCB) prototyping and low-volume production are relatively inexpensive. These tools typically can achieve routing speeds of 60 in/min or higher and spindle speeds from 20 kr/min to greater than 100 kr/min (e.g., Schmoll, T-Tech). Positional accuracies of approximately 5 (lateral) and 10 μm (vertical) are typical. The availability of end-mill diameters down to 100 μm provides the flexibility to machine a wide variety of microfluidic structures. Routing is, of course, also suitable for other materials, including many plastic films and composites. Here, we report the development of rapid prototyping of polyimide microfluidic components using micromilling and lamination and demonstrate its practicality in the fabrication of low-permeability diaphragm-based active components: fluidic capacitors and manual screw valves. XY milling of polyimide is used in conventional fabrication of circuit boards and packaging but has not previously been exploited for precision microfluidic components. In addition to describing several new machining techniques and design considerations for microfluidic devices, we also describe new lamination structures and techniques required for forming devices with internal cavities, channels, and free-standing membranes. Without these, the lamination process can create undesired plastic deformation. Finally, we describe a new vapor-cap structure which can be implemented to substantially reduce permeation of fluids through microfluidic membrane-based structures. The components are designed for a MEMS-based device for chronic infusion of drugs into the inner ear [2]. Our approach utilizes pulsatile flow to achieve drug dispersion within the cochlear fluid space. The compliant elements described in this paper provide fluidic capacitance to filter the output of a commercial miniature pump. Tuning of these capacitive elements along with series resistance optimizes flow to retain the pulsatile output but reduce the amplitude of flow-rate fluctuations. This may prevent damage to delicate cochlear structures. In addition to flow regulation, our clinical test methods require occasional switching to load test compounds delivered to the ear. The manual microvalves provide the required switching function with acceptably low leak rates. Elsewhere, we discuss the performance of the drug delivery system using these components for *in vivo* experiments [3]. This paper provides details of the fabrication and characterization of the microfabricated components.

Microfluidic devices typically have high ratios of surface area to internal volume. As a result, minimizing loss of fluid through all mechanisms, not just valve leakage, is critical. Without proper design, permeation through thin polymer layers can be the primary source of loss. A large portion of the surface of our components has low permeability because of the relatively thick walls, which are typically composed of several layers of 125-μm-thick polyimide sheets. This is not the case for the diaphragms, however. In order to achieve desired mechanical-design values (e.g., fluidic capacitance or a valve's open-state flow resistance), highly compliant layers are required. The required compliance can be achieved through either geometry, specifically area and thickness, or material choice. Increasing membrane area and decreasing thickness, both of which increase compliance, are at odds with minimizing net permeation through the structure. Similarly, with many polymers, there is some correlation between the intrinsic compliance of a material and its permeability to water and gases. One method for expanding the design space defined by these two constraints is the use of composite or layered membrane structures. Deposition of thin-film metallization onto a polymer layer reduces permeability with only moderate reduction in compliance. We have also fabricated hybrid-material devices in which the membrane is silicone, rather than polyimide. Elastomers like silicone, however, have extraordinarily high strain limits. If this high-strain capability is exercised, it precludes the use of thin-film metallization as a barrier. Even ductile metals have low strain limits in comparison and, thus, crack during use, defeating the original intended permeation-reduction function. As an alternative, we have implemented a sealed vapor chamber on the outer surface of the membrane. This vapor chamber results in substantial reduction in the steady-state fluid loss rate from the diaphragm.

II. Fabrication Methods

A. Machining

The Quickcircuit 7000 (T-Tech, Norcross, GA) XY router table was used for machining. It has a 0–60-kr/min variable spindle speed and a 0–60-in/min variable routing speed capability. Vertical-position resolution (cut-depth resolution) of the end mill is 10 μm. Double-edged clockwise-spinning stub end mills ranging from 100 to 375 μm in diameter were utilized. Rake and relief angles on these tools were estimated at 35° and 15°, respectively. Conventional cutting (finished work-piece edge is to the left, waste is to the right, relative to the direction of tool travel), as compared to climb cutting (inverse of above), yields substantially better edge quality. As a result, cutouts are routed in the clockwise direction. Similarly, for the smoothest sidewalls, channels are cut out one edge at a time, with some offset (e.g., 200-μm-diameter bit used to rout a 250-μm-width channel), rather than cut in a single pass (Fig. 1). All cuts are made with the films mounted onto a 1/8-in-thick sacrificial high-density fiberboard backer board already mounted on the router table.

Typically, we use a conservative spindle speed ranging from 10 to 20 kr/min and material feed rates of 3–6 in/min. Choosing the optimal parameters for machining of plastics is complex [20]. It is dependent on the materials and tools, and there are many competing output variables, including surface roughness, feature size and position tolerance, throughput, and tool wear. Our machining conditions are not necessarily optimized, however we conducted parametric studies varying spindle speed and feed rate and evaluated samples. The general behavior is consistent with theory [20]. At high feed rates and low spindle speeds, chip size is large, and in the extreme, results in tear out and poor edge quality, while at low feed-rate-to-spindle-speed ratios, chip size is low, and in the extreme, results in excessive heating which leads to gouging instead of clean cutting of the material.

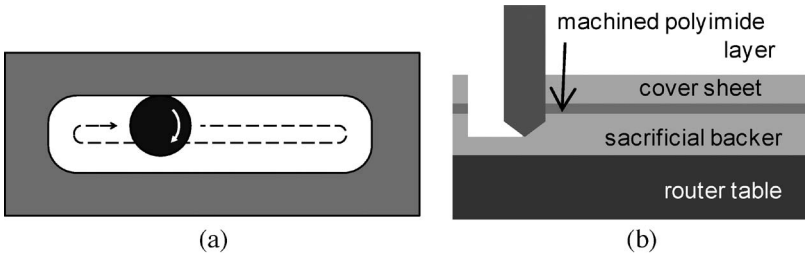

Fig. 1. (a) Milling of a channel using only conventional cutting to avoid climb cutting. The solid arrow shows the top-view rotation of the tool; the dashed arrow shows the tool path. The finished part is shaded, while the through cut is shown in white. (b) Typical material stack used for machining single layer of polyimide (cover sheet required for thin layers only).

The processes we describe have been developed using Kapton polyimide films and R/flex 1000 Kapton—adhesive laminate materials from Rogers Corporation. Specific products included the following: 1) Kapton sheets with thickness (English units used throughout text to provide consistency with manufacturer's specification) of 1 (25 μm), 3, or 5 mil; 2) laminates composed of polyimide sheets of same thickness above and 1- or 0.5-mil-thickness thermosetting adhesive; and 3) stand-alone adhesive sheets of 1-mil thickness.

The typical machining procedure for sheets or laminates with total thickness of 3 mil or more includes the following. Alignment holes in a blank sheet of desired thickness are routed. Typical alignment holes are 1/8-in diameter with 2.25-in spacing. One of the holes is oblong in the direction of the axis of the two holes, which permits expansion of the sheet during the lamination process but still provides repeatable placement of the sheet on the routing table. The sheet is then repositioned onto mating alignment pins on the router table, and the pattern is milled through the full depth of the sheet and into the backer board as shown in Fig. 1. The sides of the sheet may be taped down to improve part stability. Alternatively, vacuum stages configured with porous backer boards can be used. To machine thin layers (e.g., 1-mil polyimide or stand-alone adhesive films of 1-mil thickness or less), the mounting procedure is modified. The sheets are mounted as described earlier, but a second sacrificial layer of either 5-mil polyimide or medium tack-dicing tape is mounted on top of the layer to be machined. This provides sufficient mechanical rigidity to prevent bowing and/or tearing of the part during machining.

Finally, we describe an additional technique required to produce certain structures, including the valve seat. To prevent fallout of closed-perimeter features (islands), a partial perimeter cut is performed to leave a bridge intact. The bridge is removed with a second cut only after the island layer has been laminated to the next layer (see Section III-B as follows). This method, while it does induce some limitations on the structure shapes which can be achieved, limits the extent of double-thickness machining that might otherwise be required.

B. Cleaning

For sheets with adhesive, the adhesive backing layer is removed before cleaning. Parts are cleaned in a water-filled ultrasonic bath for 5 min. Flowing nitrogen removes excess water, and a 30-min 60-°C oven bake is used to complete the drying process. Incomplete drying can result in bubble formation in the adhesive layers and degradation of adhesion strength.

C. Lamination

1) Apparatus: The laminator consists of two chambers: a heated vacuum chamber in which the work piece is placed and an upper high-pressure chamber (420 kPaG maximum) which applies force to a movable 6-in-diameter o-ring-sealed piston between the two chambers.

2) Pressure-Relief Design: In order to fabricate devices with free-standing diaphragms using a lamination process, it is necessary to minimize pressure differentials that can develop across the diaphragm during lamination due to trapped air. Otherwise, the net pressure may cause plastic deformation. Using the same machining methods described earlier, we produce additional sheets of polyimide which are patterned with features that provide venting or pressure equilibration. These vent structures, which are stacked immediately adjacent to the active device layers during lamination, must be designed appropriately. As a rough design guideline, the pumping time constants of the volumes of air adjacent to the diaphragms (e.g., the internal and external sides of a diaphragm) should be small as compared to the pump-down time of the laminator vacuum chamber. If the pumping time constants must be small and if the volumes are large, the vent channels must have correspondingly large cross sections and short lengths. Channel lengths are largely restricted by the location of the membrane relative to the edge of the die. The width of these channels is also restricted, because they provide relief to the portion of the active layer under (or over) which they sit (see Fig. 2). This can result in localized poor lamination. In practice, it may be necessary to use a bleed valve to control the pump-down speed in combination with moderately sized vent channels. Standard formulas for hydraulic resistance of rectangular channels [21] can be applied, along with estimates of internal volumes, to arrive at appropriate design values for vent-channel dimensions.

3) Component Assembly: The stack loaded for lamination contains multiple layers in addition to the active device layers. A 0.25-in-thick aluminum base plate (typically a square with area 6.25 in^2) with alignment pins of same diameter and spacing as those used in the machining process provides the means for layer alignment. A 0.25-in-thick aluminum top plate provides uniform pressure over the parts to be laminated.

Multiple sheets of 5-mil polyimide are added to the stack as necessary to provide compliance. This compliance

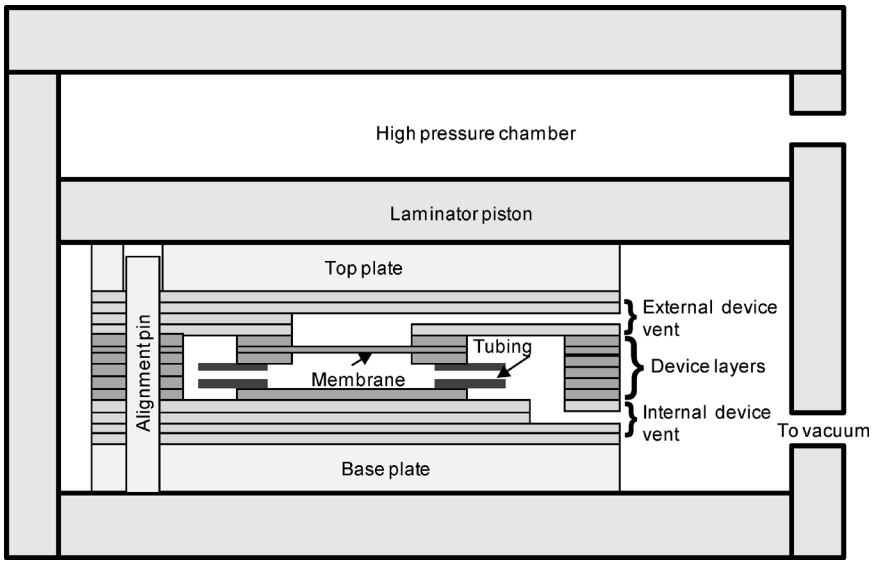

Fig. 2. Cross section of example membrane capacitor shown in lamination chamber (not to scale).

accommodates surface roughness and nonplanarity in the base and top plates, improving pressure uniformity and, hence, bond integrity. These are placed against the inner faces of the top and bottom plates in the stack and are discarded after lamination. As described earlier, additional layers of 5-mil polyimide are used for pressure equilibration. These layers are placed immediately adjacent to the top and bottom active layers of the device. Fig. 2 shows an example case of the overall stack. Note that inlet and outlet tubing may be positioned in milled grooves and included in the stack.

4) Lamination Parameters: Recommended effective lamination pressures for a particular adhesive type are achieved by setting the upper chamber pressure appropriately. Specifically, the desired adhesive lamination pressure is scaled by the ratio of the laminated-device area and the piston area to arrive at the required net laminator pressure (the gauge pressure of the upper chamber minus the vacuum level of the lamination chamber). Equivalently,

$$P_{\mathrm{set}} = P_{\mathrm{vac}} + P_{\mathrm{adh}} \frac{A_{\mathrm{die}}}{A_{\mathrm{piston}}} \tag{1}$$

where P_{set} is the upper chamber pressure setpoint, P_{vac} is the vacuum level of the lower chamber, P_{adh} is the desired lamination pressure for the adhesive, and A_{die} and A_{piston} are the areas of the laminate stack and piston. The vacuum level P_{vac} is not used to achieve the desired P_{adh}. Residual air in the lamination chamber results in bubble formation in the adhesive interfaces between polyimide layers, and thus, an appropriate vacuum level should be maintained (e.g., less than 0.5 kPa). The lamination conditions used for our typical process are shown in Table I. Parameters are consistent with the manufacturer's recommendations for R/flex 1000.

TABLE I
LAMINATION CONDITIONS

Vacuum level (kPa)	< 0.5
Over pressure (kPaG)	275
Laminate/piston area ratio ($A_{die}/A_{plunger}$)	0.2
Temperature ramp rate (°C/min)	5
Dwell time (min)	60
Dwell temperature (°C)	175
Effective adhesive pressure (P_{adh}) (kPa)	2000*

*R/flex®1000 manufacturer recommendation: 1725–2760 kPa.

D. Die Removal

Typically, two or three bridges on each edge of the die anchor it to the larger sheet. Thus, the die remains aligned in the sheet during lamination. After lamination, the die can be removed simply with knife or scissors. For high-volume production, stamp cutting may be appropriate.

E. Methods for Hybrid-Material Components

The need to produce diaphragms with both high compliance and low permeability motivates the use of hybrid-material structures. Such implementations provide the freedom to use membranes with properties different from the primary structural material making up the microfluidic component. For example, as discussed in the next section, we fabricated a capacitor mainly from polyimide but having an inserted silicone (Specialty Silicone Products SSP-M823) diaphragm. In these hybrid assemblies, additional design constraints are necessary. Specifically, the diameter of the membrane and the cutout diameters of the layers adjacent to it in the stack (layers 3 and 5 in Fig. 3) must be chosen to provide lateral strain relief of the membrane. During lamination, the membrane may be strained due to both thermal-expansion mismatch of the two materials and compression. Poor choice results in undesired buckling of the membrane. In addition, there must be sufficient overlap of the membrane and membrane-clamp layers to provide an adequate bond. Maintaining these dimensional relationships is dependent on machining tolerance. While PCB routing tools produce relatively tight dimensional tolerances for materials like polyimide, they do not work well for routing or shaping of elastomers (unless the work piece is cooled). We used biopsy

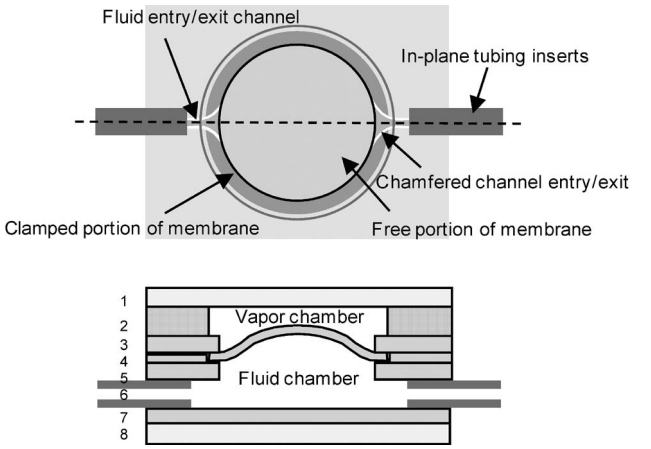

Fig. 3. Depiction of fluidic capacitor with elastomer membrane and sealed upper chamber. (upper) Top view and (lower) cross section. Layer descriptions: 1—vapor cap (glass), 2—vapor-chamber standoff, 3—upper membrane clamp, 4—membrane and membrane spacer, 5—lower membrane clamp, 6—tubing spacer layer(s), 7—bottom cap, and (optional) 8—stiffener (metal or other rigid material).

TABLE II
DESIGN VALUES FOR A SILICONE MEMBRANE IN A POLYIMIDE MICROFLUIDIC COMPONENT

Silicone membrane thickness	4 mil
Polyimide membrane spacer thickness	3 mil
Membrane diameter	5.0 mm
Membrane spacer cutout diameter (layer 4)	5.2 mm
Membrane clamp layer cutout diameters (layers 3 & 5)	4.0 mm

punches to produce circular silicone diaphragms. Example design values are provided in Table II.

In addition to choice of diaphragm material, flexibility in the choice of material and configuration of inlet and outlet ports is important. We have fabricated in-plane tubing ports using stainless steel, polyimide, and polyetheretherketone tubing. Grooves with a width typically equal to the tubing diameter are provided in the stacked layers to prevent crushing of the tubing (refer to Fig. 2).

Finally, in our current design space (i.e., component and diaphragm size ranges), either manual or pick-and-place positioning of diaphragms and tubing segments during the assembly stack-up prior to lamination is suitable. For the diaphragm design in Table II, we estimate a position-tolerance requirement of 50 μm in order to prevent gross leakage failure of the component.

F. Methods for Permeability Reduction

Depending on the material choice for the membrane, it may be so elastic (i.e., high strain limit) that thin-film metallization is not an option for permeation control, and an alternative vapor chamber may be implemented to prevent fluid loss from the structure. On the other hand, if the diaphragm is part of a valve or pump, a vapor chamber may not be viable because of interference with the component's actuation mechanism. Thus, we have chosen to develop both methods.

The structure of the vapor chamber is shown in Fig. 3. It includes a standoff or spacer and a cap layer. Both should be of low permeability (e.g., metal, glass). After lamination, the standoff, which must be of sufficient thickness to accommodate the displacement of the diaphragm at the highest operating pressure, is aligned with the diaphragm and adhered to the surrounding substrate using an appropriate adhesive. Similarly, the cap (we have used standard 8.5-mil glass microscope cover slips) is mounted and adhered. In our components, there is typically sufficient surface area present that permeability of the adhesive is not critical. We have used cyanoacrylate because it is simple to apply. In integrated systems, however, where total volume will be minimized and thus substrate area reduced, the subsequent path length of permeation through the adhesive layer will be decreased. As a result, adhesives should be chosen to minimize the product of adhesive thickness and intrinsic permeability.

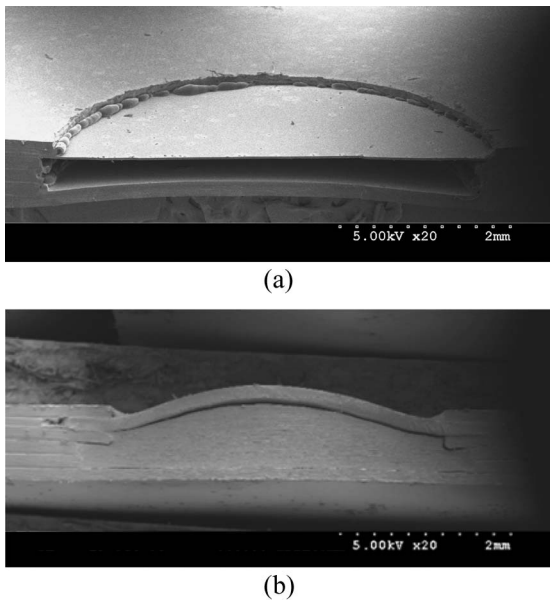

Fig. 4. Microfabricated fluidic capacitor elements. (a) 5-mm-diameter 1-mil-thickness polyimide. (b) 3.6-mm-diameter 4-mil-thickness silicone. Membrane reservoir was potted prior to sectioning to improve section cut quality.

In instances where the vapor cap is not appropriate, as is true for the manually actuated valve we describe later, thin-film metallization may be a more appropriate method for minimizing permeability. We sputter-coat diaphragms after lamination. Gold provides a good combination of ductility, corrosion resistance, and low water permeability. A thin adhesion-promoting layer of titanium or chromium (300 Å) is deposited prior to the gold deposition. Stress control of these materials is an important design consideration. Compressive films may cause undesired buckling of diaphragm structures, while highly tensile films may fatigue during device operation. Low-stress gold films were achieved in a 6-in magnetron sputter system using an applied power of 600 W and an argon pressure of 0.4 Pa. Finally, film thickness is critical. Because both permeability and compliance are inverse functions of thickness, the design space for diaphragms with low permeability and a high composite compliance is limited. For example, a 1500-Å gold layer will increase the tensile stiffness of a 1-mil polyimide membrane by 20%. Examples of several types of fabricated fluidic capacitors are shown in Fig. 4.

III. Component Design and Performance

A. Membrane Capacitor

1) Compliance: Compliant-membrane structures have been previously described [22]–[24]. In this section, we describe two example implementations of fluidic single-membrane capacitors and compare predicted differential capacitance to measured values for different membrane diameters, thicknesses, and materials.

In both cases, it is reasonable to assume a fully built-in (fixed and held) boundary condition for model purposes. The relationship between maximum displacement and applied pressure for a circular diaphragm is then given approximately by

$$\frac{Pa^4}{Et^4} = \frac{(7-\nu)\left(z^3 - z_0^3\right)}{3(1-\nu)t^3} \tag{2}$$

where P is pressure, a is membrane radius, E is tensile modulus, t is membrane thickness, v is the Poisson ratio, z is axial displacement, and z_0 is the displacement at zero applied pressure. In this section, we have modified the equation provided by Giovanni [25] by neglecting the linear bending term of $16z/[3t(1-\nu^2)]$ and by introducing an offset displacement z_0. This allows us to approximately characterize a membrane that is buckled, i.e., has a large displacement with no applied pressure. The offset displacement z_0 can be either positive or negative and will be equal in magnitude for the two cases if the membrane has a symmetric buckling tendency. As described previously, thin-film metallization of the polymer membrane can be used to achieve low permeability. The metallization, however, can induce stresses which result in buckling. In addition, the stiffness of the membrane is increased. Total volume displacement (relative to the flat unbuckled state) can be estimated from

$$V = \frac{\pi a^2 z}{2} \tag{3}$$

where it assumed that displacements are significantly greater than the membrane thickness and the membrane shape is approximately parabolic. For small displacements, where the membrane shape is approximately sinusoidal (both buckle amplitude and pressure-induced displacement are less than the diaphragm thickness), the denominator in (3) may be replaced by 1.68, and the linear term missing from (2) must be included.

An example membrane-volume-displacement plot is shown in Fig. 5. The rapid change in volume at low pressures is indicative of buckling and is a nearly symmetric function of pressure. The data set shown is that measured from a membrane with a zero-pressure buckle displacement of positive or negative 0.17 mm, as measured by a Keyence CCD Laser Displacement Sensor LK-031. $E = 3.0$ GPa (thickness-weighted average of 2.5 GPa for Kapton and 78 GPa for gold), $\nu = 0.3$, $t = 1$ mil, and $z_0 = +/-0.17$ mm were used in (2) to tabulate the displacement z as a function of applied pressure, and then, (3) was used to calculate the corresponding displacement volume shown in the model trace. The nonlinear-displacement behavior results in a large differential capacitance at low pressure that decreases rapidly with increasing pressure amplitude as shown in Fig. 6. Note that the plots in the figure represent the pressure

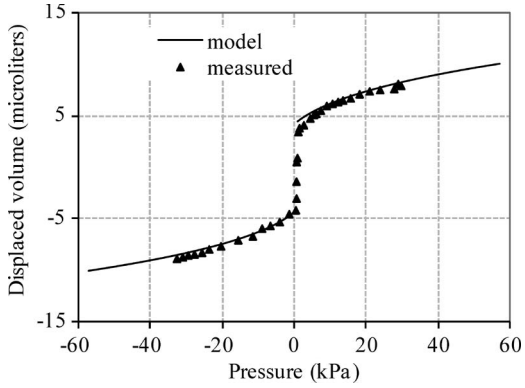

Fig. 5. Polyimide-capacitor-membrane displacement volume as a function of applied fluid pressure. Membrane has thickness of 1 mil and diameter of 8 mm. Measured buckle displacement amplitude is 0.170 mm. Displacement volume generated by a Harvard PHD2000 syringe pump. Pressure measured with an Entran Model EPX-V01 pressure transducer. Model uses $z_0 = 0.17$ mm for $P < 0$ kPa and $z_0 = -0.17$ mm for $P > 0$ kPa.

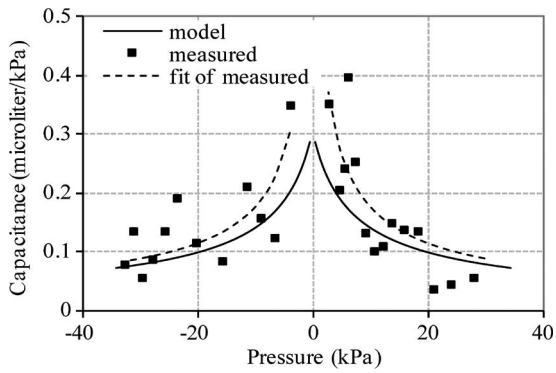

Fig. 6. Polyimide-membrane capacitance as a function of applied fluid pressure. Membrane has thickness of 1 mil and diameter of 8 mm. Buckle displacement amplitude is 0.17 mm.

derivative (taken numerically for the measured data) of the displacement volume in Fig. 5 and use no fit parameters. Also included in the figure is a best fit of the raw measured data. The fit has the form of the pressure derivative of the displacement described by (2). We believe that the discrepancy between the model and fit of the measured data results from at least two factors: the lack of precision measurement of membrane displacement, and the tendency of the buckled membrane to take on an asymmetric nonparabolic shape at low pressures.

As described earlier, our fabrication procedure provides a straightforward method for incorporating different membrane materials into the laminate-device structure. Fig. 7 shows the significant difference in volume-displacement behavior versus pressure between a thin high-modulus membrane (polyimide) and a thicker lower modulus material (silicone). As reference, for the silicone membrane, a volume displacement of 0.63 μL occurs when the axial displacement equals the diaphragm thickness of 4 mil. This is approximately where the membrane is transitioning from bending mode to tensile mode expansion (the linear and cubic terms in the displacement versus pressure equation are equal when $z/t = 1.35$ for $\nu = 0.3$). Approximately, linear behavior is observed up to this displacement volume, which occurs at 3.5 kPa. This, not incidentally, is a reasonable upper bound of operating pressure range for some

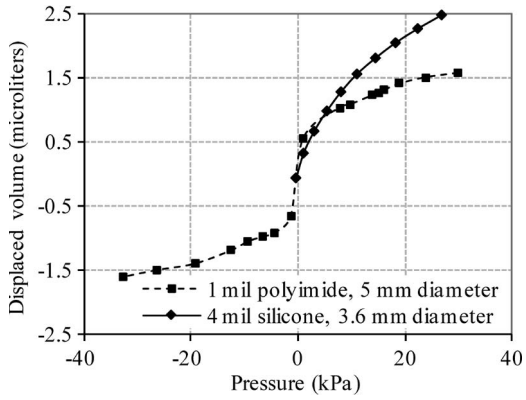

Fig. 7. Comparison between 1-mil-thick 5-mm-diameter polyimide and 4-mil-thick 3.6-mm-diameter silicone-membrane displacement volumes as a function of applied fluid pressure. Note the substantially increased nonlinearity in the polyimide membrane.

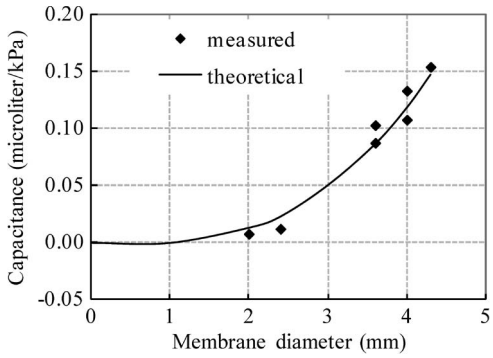

Fig. 8. Measured versus theoretical capacitance as a function of membrane diameter. Membrane material is 4-mil-thick silicone.

of the membrane capacitors in our system. The polyimide membrane, on the other hand, does not even have roughly linear-displacement volume in this pressure range.

The earlier discussion illustrates the dependence of fluid capacitance on membrane material and thickness. We also demonstrated its predictable dependence on membrane diameter. Fig. 8 shows measured small signal-capacitance values (nominal pressure is 6.9 kPa) as a function of membrane diameter using the silicone membrane. The theoretical plot was generated by taking the pressure derivative of displacement as described by (2) and then applying (3) to obtain differential volume change as a function of pressure with membrane radius as a parameter. Relatively good agreement between measured values and the design model are demonstrated.

2) Structure Permeability: As described earlier, we have implemented two methods for controlling the net loss of fluid through the thin permeable membrane: 1) for membranes with moderate strain limits (e.g., less than 3%), thin-film metallization provides a significant barrier without severely compromising compliance, and 2) for high-strain elastomers where thin-film metal coats will not be durable, a vapor cap is implemented. The vapor cap works in the following way. The vapor chamber, prior to priming of the microfluidic capacitor element, will be in equilibrium with the ambient through the permeable membrane. Once the component is primed, equilibrium is disrupted, and the relative humidity in the vapor

TABLE III
MEASURED MASS LOSS RATES FOR FOUR TYPES OF DIAPHRAGMS. ALL RATES ARE FOR WATER, ARE NORMALIZED TO MEMBRANE AREA, AND HAVE UNITS OF MICROGRAM/DAY/mm^2

1 mil thick polyimide	34
1 mil thick polyimide with Ti/Au (300, 1500Å) film	12
4 mil thick silicone	640
4 mil thick silicone with glass vapor cap	14

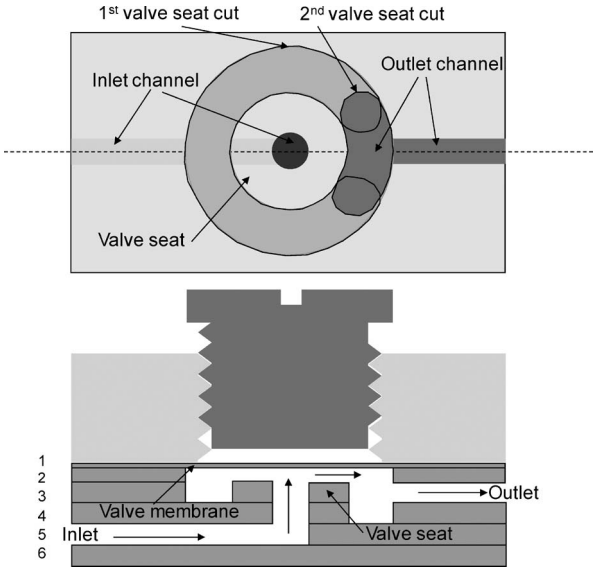

Fig. 9. Depiction of normally open screw valve. (upper) Top view and (lower) cross section. Layers 3 and 4 are laminated together between the first and second valve-seat cuts.

chamber rises toward 100%. At this point, net transport through the membrane stops, and as a result, the capacitor stops losing fluid (assuming that the vapor chamber is well sealed). Maintaining this equilibrium condition, however, requires a constant temperature. If temperature increases, the relative humidity in the vapor chamber will decrease, and water will move from the liquid to vapor side of the membrane until the 100% relative humidity condition is again achieved. This represents a net loss of fluid from the fluidic portion of the component. Alternatively, if the temperature drops, condensation will occur in the vapor chamber. An effective seal on the vapor chamber is critical, particularly in drug delivery applications where dose tolerances are tight. Leakage can result in both an undesired change in concentration of drug delivered to the target site and delivery of drug to an undesired location. Table III lists measured mass-loss rates for various water-filled membrane-capacitor structures at ambient pressure and temperature. Mass loss was measured by capping the component ports with a fitting known to have negligible permeability and, then, recording the change in total mass at intervals over several days.

B. Manual Screw Valve

In addition to fluid capacitors, we have also designed, built, and measured the performance of a manually actuated screw valve. Manual microfluidic screw valves were demonstrated by the Whitesides group [26], but the screw acted by direct

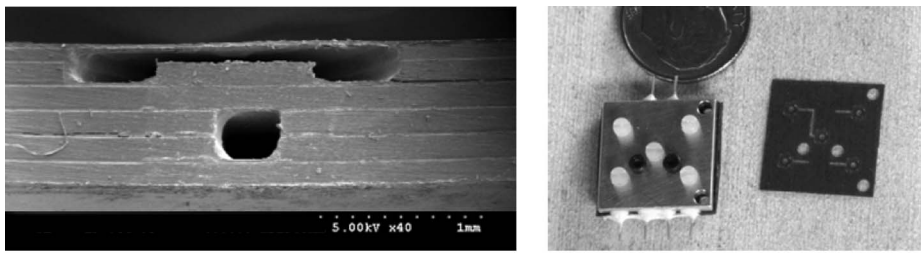

Fig. 10. (a) SEM cross section (section is slightly offset from centerline of valve) of valve structure and (b) micrograph of valve manifold with nylon screw actuation.

compression on a silicone channel. Our implementation uses a laminate structure with a ring-shaped valve seat and a membrane, as shown in Fig. 9. Axial displacement of the screw forces the membrane into contact with the valve seat and restricts flow between the inlet channel, which terminates at the inner diameter of the seat, and the outlet channel, which takes the form of a torus surrounding the valve seat. As described earlier, there are two valve-seat cuts which define the valve-seat perimeter and the torus portion of the outlet channel. The first valve-seat cut defines approximately 330° of the seat perimeter. After lamination to the channel spacer layer, the second valve-seat cut defines the remaining 30° of the seat perimeter.

As with the microfluidic capacitors, these valves can be built with different membrane materials and in arbitrary configurations within a larger manifold of components. A five-valve manifold was designed for similar functionality to a high-performance liquid chromatography injection valve and was manufactured in a 1.5 cm × 1.5 cm die format with top and bottom aluminum plates as shown in Fig. 10. Holes in the top plate aligned with valve seats are tapped to provide placement for the actuation screws. The bottom plate is used in high-pressure applications where large axial screw forces must be applied. Coupling the plates with clamping bolts prevents delamination of the top plate from the laminate stack.

Two screw types have been examined. The first is a steel 0–80 hex socket set screw with a cup point. The diameter of the cup point is matched to the nominal diameter of the valve seat. While this provides a very high effective pressure on the membrane during valve closure, it has a relatively small contact area requiring precise alignment of the aluminum top plate to the polyimide stack. In addition, it generates wear on the outer surface of the membrane, severely limiting the cycle count of the valve. The second screw type is a nylon 0–80 slotted-head screw with a flat tip. This generates approximately uniform pressure over the valve seat and, because of the better match in material hardness between nylon and polyimide (or silicone), generates significantly less wear on the membrane. Given that our system's internal fluid volume is approximately 100 μL and our experiment duration can approach several months, low leak rates are required. Open-state resistance and closed-state leak rates for multiple polyimide-diaphragm valves using nylon screws to control water flow are listed in Table IV. Silicone-diaphragm valves were also fabricated; however, performance was erratic due to intermittent sticking of the diaphragm to the valve seat. Open-state resistances were calculated from the slope of a linear fit of measured flow rate versus pressure set point, with at least five different set points ranging from 0 to 50 kPa. Closed-state leak rates were measured at a pressure set point of 100 kPa. Flow rates in both cases were determined by measurement of linear displacement over time of a water slug traveling through fine-bore tubing attached to the output port of the valve under test. We have also explored the use of these valves as manually operated flow restrictors. Flow rate as a function of screw displacement is shown in Fig. 11. Finally, no significant hysteresis was observed, as observed by the good repeatability of the valve conduction through two cycles of opening and closing.

TABLE IV
MEASURED VALVE CHARACTERISTICS USING NYLON SCREWS

Leak rate at 100 kPa (1 in·ounce applied torque) (μL/min)*	0.015 – 0.040
Resistance in open position (kPa·min/μL)†	0.028 - 0.065
Minimum resistance ratio, Closed:Open	> 38 000

*- 3 valves tested, † - 5 valves tested

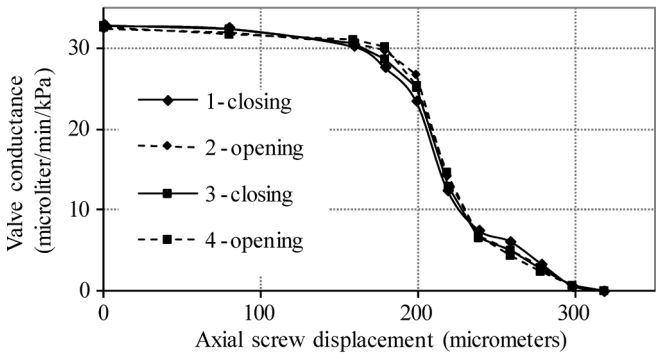

Fig. 11. Manual screw valve. Water conductance versus axial screw displacement using 0–80 nylon screw. Pressure across entire test system including inlet and outlet was held at approximately 28 kPa. The screw first engages the valve membrane at approximately 100-μm displacement.

IV. CONCLUSION

In this paper, we have demonstrated low-permeability diaphragm-based components developed for a microfluidic drug delivery system. We have developed a set of versatile fabrication techniques suitable for rapid prototyping of laminate-based polymer microfluidic systems. Two methods for reducing the permeability of polymer-based microfluidic components have been demonstrated. Given the many advantages of polymer systems, the components and techniques described should

prove useful for a broad range of microfluidic applications, including drug delivery systems.

ACKNOWLEDGMENT

The authors would like to thank E. Kim and C. Cardoso for their contributions. The contents of this paper are solely the responsibility of the authors and do not necessarily represent the official views of the NIDCD.

REFERENCES

[1] M. C. Holley, "The auditory system, hearing loss and potential targets for drug development," *Drug Discov. Today*, vol. 10, no. 19, pp. 1269–1282, Oct. 2005.

[2] Z. Chen, S. G. Kujawa, M. J. McKenna, J. O. Fiering, M. J. Mescher, J. T. Borenstein, E. E. L. Swan, and W. F. Sewell, "Inner ear drug delivery via a reciprocating perfusion system in the guinea pig," *J. Control. Release*, vol. 110, no. 1, pp. 1–19, Dec. 2005.

[3] J. Fiering, M. J. Mescher, E. E. L. Swan, M. E. Holmboe, B. A. Murphy, Z. Chen, M. Peppi, W. F. Sewell, M. J. McKenna, S. G. Kujawa, and J. T. Borenstein, "Local drug delivery with a self-contained, programmable, microfluidic system," *Biomed. Microdevices*, vol. 11, no. 3, Jun. 2009.

[4] H. Becker and C. Gartner, , "Polymer microfabrication methods for microfluidic analytical applications," *Electrophoresis*, vol. 21, no. 1, pp. 12–26, Jan. 2000.

[5] B.-H. Jo, L. M. V. Lerberghe, K. M. Motsegood, and D. J. Beebe, "Three-dimensional micro-channel fabrication in polydimethylsiloxane (PDMS) elastomer," *J. Microelectromech. Syst.*, vol. 9, no. 1, pp. 76–81, Mar. 2000.

[6] Y. Xia and G. M. Whitesides, "Soft lithography," *Annu. Rev. Mater. Sci.*, vol. 28, no. 1, pp. 153–184, Aug. 1998.

[7] L. J. Guerin, M. Bossel, M. Demierre, S. Calmes, and P. Renaud, "Simple and low cost fabrication of embedded micro-channels by using a new thick-film photoplastic," in *Proc. Solid State Sens. Actuators*, Chicago, IL, 1997, pp. 1419–1422.

[8] L. Martynova, L. E. Locascio, M. Gaitan, G. W. Kramer, R. G. Christensen, and W. A. MacCrehan, "Fabrication of plastic microfluidic channels by imprinting methods," *Anal. Chem.*, vol. 69, no. 23, pp. 4783–4789, Dec. 1, 1997.

[9] H. Becker and U. Heim, "Hot embossing as a method for the fabrication of polymer high aspect ratio structures," *Sens. Actuators A, Phys.*, vol. 83, no. 1–3, pp. 130–135, May 2000.

[10] W. K. Schomburg, R. Ahrens, W. Bacher, J. Martin, and V. Saile, "AMANDA—Surface micromachining, molding, and diaphragm transfer," *Sens. Actuators A, Phys.*, vol. 76, no. 1–3, pp. 343–348, Aug. 30, 1999.

[11] T. Rogge, Z. Rummler, and W. K. Schomburg, "Polymer microvalve with hydraulic piezo-drive fabricated by the AMANDA process," *Sens. Actuators A, Phys.*, vol. 110, no. 1–3, pp. 206–212, Feb. 1, 2004.

[12] A. Wego, S. Richter, and L. Pagel, "Fluidic microsystems based on printed circuit board technology," *J. Micromech. Microeng.*, vol. 11, no. 5, pp. 528–531, Sep. 2001.

[13] S. Metz, R. Holzer, and P. Renaud, "Polyimide-based microfluidic devices," *Lab Chip*, vol. 1, no. 1, pp. 29–34, 2001.

[14] S. Metz, C. Trautmann, A. Bertsch, and P. Renaud, "Polyimide microfluidic devices with integrated nanoporous filtration areas manufactured by micromachining and ion track technology," *J. Micromech. Microeng.*, vol. 14, no. 3, pp. 324–331, Mar. 2004.

[15] G. Zhang, V. Chu, and J. Conde, "Electrostatically actuated bilayer polyimide-based microresonators," *J. Micromech. Microeng.*, vol. 17, no. 4, pp. 797–803, Apr. 2007.

[16] E. Lindner, V. V. Cosofret, S. Ufer, R. P. Buck, R. P. Kusy, R. B. Ash, and H. T. Nagle, "Flexible (Kapton-based) microsensor arrays of high stability for cardiovascular applications," *J. Chem. Soc., Faraday Trans.*, vol. 89, pp. 361–367, 1993.

[17] P. M. Martin, D. W. Matson, W. D. Bennett, Y. Lin, and D. J. Hammerstrom, "Laminated plastic microfluidic components for biological and chemical systems," *J. Vac. Sci. Technol. A, Vac. Surf. Films*, vol. 17, no. 4, pp. 2264–2269, Jul. 1999.

[18] M. J. Mescher, C. E. Dube, M. Varghese, and J. O. Fiering, "Surface mount microfluidic flow regulator on a polymer substrate," in *Proc. MicroTAS*, Squaw Valley, CA, 2003, pp. 947–950.

[19] C. E. Dubé, J. O. Fiering, and M. J. Mescher, "A Si-based FPW sensor array system with polymer microfluidics integrated on a PCB," in *Proc. IEEE Sensors*, Orlando, FL, 2002, pp. 460–465.

[20] A. Kobayashi, *Machining of Plastics*. Huntington, NY: Krieger, 1981. Reprinted from 1967 edition.

[21] N.-T. Nguyen and S.T. Wereley, *Fundamentals and Applications of Microfluidics*. Boston, MA: Artech House, 2002.

[22] C. J. van Mullem, K. J. Gabriel, and H. Fujita, "Large deflection performance of surface micromachined corrugated diaphragms," in *Proc. TRANSDUCERS*, San Francisco, CA, 1991, pp. 1014–1017.

[23] R. Miles and D. L. Schumann, "Thin-walled compliant plastic structures for meso-scale fluidic systems," in *Proc. SPIE Conf.: Micro- Nanofabricated Struct. Devices Biomed. Environ. Appl. II*, San Jose, CA, 1999, pp. 129–136.

[24] B. Yang, J. Metter, and Q. Lin, "Using compliant membranes for dynamic flow stabilization in microfluidic systems," in *Proc. 18th IEEE Int. Conf. Micro Electro Mech. Syst.*, 2005, pp. 706–709.

[25] M. D. Giovanni, *Flat and Corrugated Diaphragm Design Handbook*. New York: Marcel Dekker, 1982.

[26] D. B. Welbel, M. Kruithof, S. Potenta, S. K. Sia, A. Lee, and G. M. Whitesides, "Torque-actuated valves for microfluidics," *Anal. Chem.*, vol. 77, no. 15, pp. 4726–4733, Aug. 1, 2005.

Mark J. Mescher received the B.S. degree in computer engineering from Wright State University, Dayton, OH, in 1993, and the M.S. and Ph.D. degrees in electrical engineering from Carnegie Mellon University, Pittsburgh, PA, in 1995 and 1999, respectively.

He is currently a Principal Member of the Technical Staff at Charles Stark Draper Laboratory, Cambridge, MA, in the MEMS design group, where his focus areas include microfluidic system development and MEMS components for precision timing applications. He worked previously at Sandia National Laboratory.

Erin E. Leary Swan received the B.S. degree in aerospace engineering from the Pennsylvania State University and the M.S. degree in biomedical engineering from Boston University, Boston, MA. She is a Draper Fellow and working toward the Sc.D. degree in mechanical engineering at Massachusetts Institute of Technology, Cambridge.

She previously served as an officer in the United States Navy. Her research interests include microfluidic drug delivery systems and tissue engineering.

Jason Fiering received the B.A. degree in physics from Wesleyan University, Middletown, CT, in 1990, and the M.S. degree in physics from Duke University, Durham, NC, in 1996.

He has been a Research Associate in microfabrication and device design at AT&T Bell Laboratories, Murray Hill, NJ, Duke University, and North Carolina State University. He is currently a Senior Member of the Technical Staff at Charles Stark Draper Laboratory, Cambridge, MA, where his focus is on microfluidic systems for biomedical applications and on polymer microfabrication.

Maria E. Holmboe received the B.S. degree in earth and geographical sciences with a minor in mathematics from the University of Massachusetts, Boston, in 2003.

She is currently a Member of the Technical Staff at Charles Stark Draper Laboratory, Cambridge, MA, in the Biomedical Engineering group, where her focus areas include microfluidic components development and fielded biosensor applications.

William F. Sewell received the Ph.D. degree in pharmacology from Tulane University, New Orleans, LA, in 1978.

He completed a fellowship in the Research Laboratory of Electronics, Massachusetts Institute of Technology, Cambridge, in 1982. He then joined the faculty at Harvard Medical School, Boston, MA, where he is an Associate Professor of Otolaryngology. His laboratory is at the Massachusetts Eye and Ear Infirmary, Boston.

Sharon G. Kujawa received the Ph.D. degree in audiology (focus on hearing science/pharmacology) from the University of Arizona, Tucson.

She completed postdoctoral fellowships in auditory pharmacology at the Kresge Hearing Research Laboratory, New Orleans, LA, and in auditory neurophysiology at the Eaton-Peabody Laboratory, Boston, MA.

Currently, she is an Associate Professor of Otology and Laryngology, Harvard Medical School, Boston, and Director of the Department of Audiology at the Massachusetts Eye and Ear Infirmary, Boston. She is on the faculty of the Harvard-MIT Program in Speech and Hearing Biosciences and Technology and is a Principal Investigator in the Eaton-Peabody Laboratory of the Massachusetts Eye and Ear Infirmary.

Michael J. McKenna received the B.A. degree from the University of California, San Diego, and the M.D. degree from the University of Southern California School of Medicine, Los Angeles, in 1982.

He is currently a Professor of Otology and Laryngology at the Harvard Medical School, Boston, MA, and a Surgeon in Otolaryngology, Division of Otology, Massachusetts Eye and Ear Infirmary, Boston.

Dr. McKenna is a member of the American Medical Association, American College of Surgeons, American Neurotology Society, American Otological Society, Otosclerosis Study Group, Collegium Oto-Rhnio-Laryngologicum, Massachusets Medical Society, and the American Academy of Otolaryngology.

Jeffrey T. Borenstein was born in Baton Rouge, LA. He received the B.S., M.S., and Ph.D. degrees in physics from the University at Albany, NY, while simultaneously working at North American Philips Corporation on the development of novel electronic materials for the semiconductor industry.

He is currently a Distinguished Member of the Technical Staff at the Charles Stark Draper Laboratory, Cambridge, MA. Prior to joining Draper Laboratory he was Solar Cell Fabrication Manager at a division of Mobil Oil Corporation. He is the holder of 13 issued patents and another 19 patent applications in the fields of MEMS fabrication technology, inertial MEMS sensors, tissue engineering, and drug delivery. He has supervised six M.S. and six Ph.D. students at Massachusetts Institute of Technology and currently directs several programs developing new technologies for the pharmaceutical and medical device industries. His current research interests focus on the development of tools for drug discovery, organ assist devices, and implantable drug delivery systems.